DATA-DRIVEN MODEL DISCOVERY AND CONTROL OF HIGH-PERFORMANCE TRAINER AIRCRAFT VIA SPARSE IDENTIFICATION OF NONLINEAR DYNAMICS

Minwoo Kang[1], Jayden Dongwoo Lee[2], Seonghun Yun[1] & Hyochoong Bang[2]

[1]ADD, Daejeon, Republic of Korea
[2]KAIST, Daejeon, Republic of Korea

Abstract

This paper presents an application of data-driven modeling and control for the dynamics of a fixed-wing aircraft. Sparse identification of nonlinear dynamics (SINDy) and least square method (LSM) are used to obtain a data-driven aircraft model. Using the data-driven model, attitude control simulations are performed using nonlinear model predictive control (NMPC). Simulation results demonstrate that the data-driven model using SINDy can represent aerodynamic nonlinearities compared to the model using LSM. This difference leads to significant performance improvements in the NMPC.

Keywords: Fixed-Wing Aircraft, SINDy, System Identification, Data-Driven Modeling, Model Predictive Control

1. Introduction

Uncertainty in models due to nonlinearities remains an unresolved challenge in the field of aeronautics. This is because the nature of aircraft model uncertainty results from unexpected or unpredictable conditions caused by various features. Those small model uncertainties can even cause serious fatigue to pilots in flight control, and if combined with human errors, such as unskilled pilots, catastrophic disasters can occur. The aerodynamic model, one of the sources of uncertainty, significantly impacts aircraft. Therefore, in conventional aircraft, it is common to define the stall envelope based on the angle of attack, where nonlinear aerodynamics occurs. In addition, multiple safety mechanisms are implemented to avoid reaching the stall angle of attack regions [1].

Special aircraft that require high-performance need to make steep maneuvers, such as entering the stall envelope. Therefore, knowing exactly the aerodynamic force in the stall envelope is a highly important task in terms of flight stability. Consequently, it can affect the margin design of the flight control system [2, 3]. However, there have been wind tunnel tests and computational fluid dynamics to determine the aerodynamic characteristics of aircraft, all of which have a gap with the aerodynamic characteristics of the full model of the aircraft just before the actual flight. [4, 5].

As a solution to these problems, there is a system identification technique using data, which is a rapidly evolving field called data-driven modeling [6, 7]. In particular, the method is useful for discovering the dynamics of nonlinear systems that are difficult to model in advance through engineering schemes.

Neural networks are implemented using massive connections among processing units with variable strengths, and it is attractive for applications in system identification and control [8]. Gaussian process (GP) is widely used in system modeling and control of dynamic systems because of its non-parametric characteristic and the advantage that it works properly in noisy, uncertain situations [9, 10]. Koopman operator theory, which is the principal linear embedding of nonlinear dynamics, has recently emerged as the leading framework to identify nonlinear dynamical systems from data [11].

The least square method (LSM) is a parameter estimation method based on minimizing the sum of the squares of the residuals from the results of each individual equation in a regression analysis.

LSM is a powerful tool for handling big data for regression and fitting to linear models. These characteristics lead to the usage of LSM in an estimation of aircraft coefficients [12] through flight data. It shows that LSM can estimate the aerodynamic coefficients in every axis, assuming the structure of the aerodynamic model is known.
Sparse identification for nonlinear dynamics (SINDy) is a data-driven model discovery framework, one of the emerging system identification methods using sparse regression [13, 14, 15]. This method, which extracts only the key state of the nonlinear model from the candidate function through sparsity-promoting optimization, can estimate the governing equation of the nonlinear target model [16]. Also, SINDy is implemented in the quadrotor system, including the gyroscopic and aerodynamic effect to find a governing equation [17]. For the convenience of SINDy, it is chosen as the data-driven method for this research. LSM is also used to compare with SINDy and to validate itself. Therefore, the aim of this paper is to compare two data-driven methods for aircraft and implement a nonlinear model predictive control (NMPC) by data-driven models to improve flight performance.
The remainder of the paper is arranged as follows: Section 2 introduces aircraft dynamics and model configurations. Section 3 explains the methodology for applying data-driven methods to the discovery of aircraft dynamics. Section 4 presents a process and results of data-driven modeling with LSM and SINDy. Furthermore, Section 5 shows flight simulation results using the discovered model with NMPC. Finally, Section 6 gives the conclusions.

2. Problem Formulation

2.1 Aircraft Dynamics

2.1.1 Motion & Kinematic Equation Modeling

Aerodynamic forces and moments in the body-fixed coordinate are expressed as $[F_{x,Aero}, F_{y,Aero}, F_{z,Aero}]$ and $[L_{Aero}, M_{Aero}, N_{Aero}]$, respectively. On the same axis, velocity and angular velocity are described as $[U,V,W]$ and $[p,q,r]$. ϕ and θ represent roll angle and pitch angle, which refers to the angle of attitude of the aircraft defined as the difference between the body-fixed coordinate and the earth-fixed coordinate. T means the thrust of the engine assumed to be parallel to the x-axis in body-fixed coordinate. Finally, m and $[I_{xx}, I_{yy}, I_{zz}]$ represent the mass and moment of inertia of aircraft. Assuming a conventional symmetrical configuration, 6-DOF motion equations of fixed-wing aircraft [14, 15, 18] are given in (1) to (6),

$$F_{x,Aero} = m(\dot{U} - Vr + Wq + gsin\theta) - T, \tag{1}$$

$$F_{y,Aero} = m(\dot{V} + Ur - Wp - gsin\phi cos\theta), \tag{2}$$

$$F_{z,Aero} = m(\dot{W} - Uq + Vp - gcos\phi cos\theta), \tag{3}$$

$$L_{Aero} = I_{xx}\dot{p} + (I_{zz} - I_{yy})qr, \tag{4}$$

$$M_{Aero} = I_{yy}\dot{q} + (I_{xx} - I_{zz})pr, \tag{5}$$

$$N_{Aero} = I_{zz}\dot{r} + (I_{yy} - I_{xx})pq. \tag{6}$$

And kinematic equations are as follows:

$$\dot{\phi} = p + qsin\phi tan\theta + rcos\phi tan\theta, \tag{7}$$

$$\dot{\theta} = qcos\phi - rsin\phi. \tag{8}$$

Aerodynamic models consist of variables with α, β which describe angle of attack and angle of sideslip in the wind axis coordinate. These can replace V and W in (1) to (3) below:

$$\alpha = tan^{-1}(\frac{W}{U}) \leftrightarrow W = Utan\alpha, \tag{9}$$

$$\beta = tan^{-1}(\frac{V}{U}) \leftrightarrow V = Utan\beta. \tag{10}$$

$$\dot{W} \cong U\dot{\alpha}sec^2\alpha, \tag{11}$$

$$\dot{V} \cong U\dot{\beta}sec^2\beta. \tag{12}$$

Therefore, (1) to (3) become as:

$$F_{x,Aero} = m(\dot{U} - rUtan\beta + qUtan\alpha + gsin\theta) - T, \tag{13}$$

$$F_{y,Aero} = m(U\dot{\beta}sec^2\beta + Ur - pUtan\alpha - gsin\phi cos\theta), \tag{14}$$

$$F_{z,Aero} = m(U\dot{\alpha}sec^2\alpha - Uq + pUtan\beta - gcos\phi cos\theta). \tag{15}$$

2.1.2 Aerodynamic Equation Modeling

The aerodynamic force and moment can be explained as the sum of stability derivative terms and control derivative terms. Each term is gathered from aerodynamic analysis methods such as wind tunnel tests and computational fluid dynamics simulations.

The aerodynamic data utilized in this research originates from internal sources via wind tunnel testing. The initial raw data is presented as a look-up table containing numerous data points. The look-up table format is reorganized to a non-linear function format in order to focus on the identification of non-linear dynamics as the main topic of this research. Therefore, the aerodynamic force and moment equation is expressed as the linear combination of various non-linear state terms as follows:

$$F_{x,Aero} = (\hat{C}_L sin\alpha - \hat{C}_D cos\alpha)\bar{q}S_w, \quad F_{y,Aero} = \hat{C}_Y \bar{q}S_w, \quad F_{z,Aero} = (-\hat{C}_L cos\alpha - \hat{C}_D sin\alpha)\bar{q}S_w, \tag{16}$$

$$L_{Aero} = (\hat{C}_r cos\alpha - \hat{C}_n sin\alpha)\bar{q}S_w b, \quad M_{Aero} = \hat{C}_m \bar{q}S_w \bar{c}, \quad N_{Aero} = (\hat{C}_r sin\alpha + \hat{C}_n cos\alpha)\bar{q}S_w b, \tag{17}$$

where,

$$\hat{C}_D = f(1, \alpha, \alpha^2, \beta^2, \alpha^3, \alpha^4, \alpha^5, \delta_{ele}, \alpha\delta_{ele}, \delta_{rud}^2, \beta\delta_{rud}^2), \tag{18}$$

$$\hat{C}_Y = f(\beta, \alpha\beta, \beta^3, \alpha\beta^3, \beta^5, \delta_{rud}, \beta\delta_{rud}) + C_{Y_p}\frac{bp}{2V_T}, \tag{19}$$

$$\hat{C}_L = f(1, \alpha, \alpha^3, \alpha\beta^2, \alpha^5, \alpha^3\beta^2, \delta_{ele}, \alpha\delta_{ele}) + C_{L_q}\frac{\bar{c}q}{2V_T}, \tag{20}$$

$$\hat{C}_r = f(\beta, \alpha\beta, \beta^2, \alpha\beta^3, \alpha^4\beta, \alpha^2\beta^3, \delta_{ail}, \beta\delta_{ail}, \delta_{rud}, \beta\delta_{rud}) + C_{r_p}\frac{bp}{2V_T} + C_{r_r}\frac{br}{2V_T}, \tag{21}$$

$$\hat{C}_m = f(1, \alpha, \alpha^2, \alpha^3, \alpha\beta^2, \alpha^4, \alpha^2\beta^2, \alpha\beta^4, \delta_{ele}, \alpha\delta_{ele}) + C_{m_q}\frac{\bar{c}q}{2V_T}, \tag{22}$$

$$\hat{C}_n = f(\beta, \alpha\beta, \beta^2, \beta^3, \alpha\beta^3, \beta^4, \beta^5, \delta_{ail}, \beta\delta_{ail}, \delta_{ail}^2, \delta_{rud}, \beta\delta_{rud}) + C_{n_p}\frac{bp}{2V_T} + C_{n_r}\frac{br}{2V_T}, \tag{23}$$

with

$$\begin{aligned} \bar{q} &= \frac{1}{2}\rho V_T^2, \\ V_T &= \sqrt{U^2 + V^2 + W^2}. \end{aligned} \tag{24}$$

$\hat{C}_O$ refers to the non-linear aerodynamic coefficients for brevity. $[\hat{C}_D, \hat{C}_Y, \hat{C}_L]$ and $[\hat{C}_r, \hat{C}_m, \hat{C}_n]$ are force and moment coefficients of X, Y, Z axis defined in stability coordinate. Each of ρ, S_w, $\bar{c}$, b represents the air density, reference wing area, mean aerodynamic chord length, and wing span of the aircraft. Substituting (16) and (17), the dynamic model can have a form of the differential equation like (25) to (30).

$$\dot{U} = \frac{\hat{C}_L sin\alpha - \hat{C}_D cos\alpha}{m}\bar{q}S_w - gsin\theta + \frac{T}{m} - qW - rV, \tag{25}$$

$$\dot{\beta} = (\frac{\hat{C}_Y \bar{q}S_w}{m} + gcos\theta sin\phi - rU - pW)\frac{cos^2\beta}{U}, \tag{26}$$

$$\dot{\alpha} = (\frac{-\hat{C}_L cos\alpha - \hat{C}_D sin\alpha}{m}\bar{q}S_w + gcos\theta cos\phi - pV - qU)\frac{cos^2\alpha}{U}, \tag{27}$$

$$\dot{p} = \frac{(\hat{C}_r cos\alpha - \hat{C}_n sin\alpha)\bar{q}S_w b - (I_{zz} - I_{yy})qr}{I_{xx}}, \tag{28}$$

$$\dot{q} = \frac{\hat{C}_m \bar{q}S_w \bar{c} - (I_{xx} - I_{zz})rp}{I_{yy}}, \tag{29}$$

$$\dot{r} = \frac{(\hat{C}_r sin\alpha + \hat{C}_n cos\alpha)\bar{q}S_w b - (I_{yy} - I_{xx})pq}{I_{zz}}. \tag{30}$$

2.2 Aircraft Model Configuration

In this study, a Korean single-turboprop two-seat trainer aircraft, KT-1 in Figure 1 is selected as the model for simulation and analysis. The specifications and configurations of this aircraft [19] are as follows in Table 1.

Figure 1 – KT-1 prototype in Korea war-memorial organization exhibition.

Length [m]	10.26
Wingspan [m]	10.59
Aspect ratio	7
Wing area [m^2]	16.01
Gross weight [kg]	2,450
Powerplant	Pratt & Whitney Canada PT6A-62 turboprop engine

Table 1 – Detail characteristics of KT-1.

There are some advantages to choosing a conventional trainer aircraft as the target model. First, it is possible to prove the validity of the estimated model from system identification. Both precise dynamic models and flight data are essential for reliable system identification. If you select a small fixed-wing UAV as the target aircraft, it might be easy to measure flight data through a real flight test. However, it would be hard to validate the reliability of the estimated model because of the lack of a ground truth model as a comparison model. With trainer aircraft, almost true flight data can be gathered through sophisticated simulation models via an accurate aerodynamic model from numerous wind tunnel tests. Additionally, it is appropriate for testing non-linear coupled flight phases like a high-maneuver since the performance of the identification method is determined by how robust they are in the non-linear region.

3. Data Driven Model Discovery Methods

3.1 Sparse Identification of Nonlinear Dynamics

In recent times, while machine learning modeling techniques have found extensive applications across various engineering domains, they often fail to offer a significant representation of the system and require substantial data to train the model. The SINDy method, however, has the benefit of deriving governing equations for target systems with less data compared to traditional deep neural networks. The main concept is to identify a sparse model from a set of candidate functions, under the assumption that a few functions with dominant system characteristics. Then, to obtain the sparse model, we consider the continuous-time nonlinear system

$$\dot{\mathbf{X}} = \Theta(\mathbf{X}, \mathbf{U})\Xi, \tag{31}$$

where Ξ is the coefficient of the model, Θ is the library of the candidate functions and $\dot{\mathbf{X}}$ is the time derivative of the state.

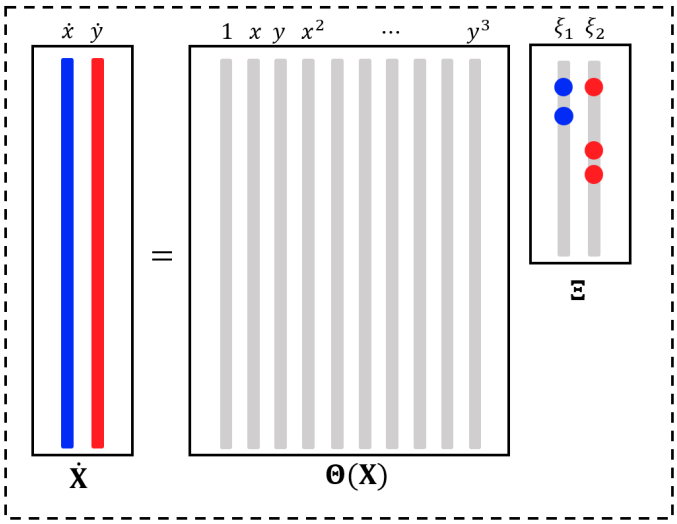

Figure 2 – Concept of SINDy.

To find the sparse model, we collect the sequential data of state to make the snapshots of state and control input as:

$$\mathbf{X} = \begin{bmatrix} x_1(t_1) & x_2(t_1) & \cdots & x_n(t_1) \\ x_1(t_2) & x_2(t_2) & \cdots & x_n(t_2) \\ \vdots & \vdots & \ddots & \vdots \\ x_1(t_m) & x_2(t_m) & \cdots & x_n(t_m) \end{bmatrix}, \tag{32}$$

$$\mathbf{U} = \begin{bmatrix} u_1(t_1) & u_2(t_1) & \cdots & u_n(t_1) \\ u_1(t_2) & u_2(t_2) & \cdots & u_n(t_2) \\ \vdots & \vdots & \ddots & \vdots \\ u_1(t_m) & u_2(t_m) & \cdots & u_n(t_m) \end{bmatrix}. \tag{33}$$

If we do not measure this value directly by the sensor, we should use a numerical differential method to obtain the state's time derivative.

$$\dot{\mathbf{X}} = \begin{bmatrix} \dot{x}_1(t_1) & \dot{x}_2(t_1) & \cdots & \dot{x}_n(t_1) \\ \dot{x}_1(t_2) & \dot{x}_2(t_2) & \cdots & \dot{x}_n(t_2) \\ \vdots & \vdots & \ddots & \vdots \\ \dot{x}_1(t_m) & \dot{x}_2(t_m) & \cdots & \dot{x}_n(t_m) \end{bmatrix}. \tag{34}$$

The library of candidate functions is designed including any type of function such as polynomial, trigonometric, and exponential functions. If we know the prior information of the system, some functions are utilized in the library of candidate functions to enhance the model accuracy.

$$\Theta(\mathbf{X},\mathbf{U}) = \begin{bmatrix} | & | & | & | & | & | & | \\ \mathbf{1} & \mathbf{X} & \mathbf{U} & \mathbf{X}\otimes\mathbf{X} & \cdots & sin(\mathbf{X}) & \cdots \\ | & | & | & | & | & | & | \end{bmatrix}. \tag{35}$$

where $x \otimes y$ defines the vector of all product combinations of the components in x and y.
In the regression problem, L_1 regularization promotes a sparse solution in the coefficient Ξ_k which is an element of Ξ. We use a sequential threshold least square algorithm (STLS) [13] to obtain a sparse aircraft parameter. The sparse regression problem is formulated as follows:

$$\Xi_k = \arg\min \left\| \dot{X}_k - \Theta(\mathbf{X},\mathbf{U})\Xi_k \right\|_2^2 + \lambda \left\| \Xi_k \right\|_1, \tag{36}$$

where λ is the regularization parameter that induces sparsity as L_1 penalty.

3.2 Least Square Method

Assuming that the true structure of a dynamic model is known, the general least square method (LSM) can be applied to estimate the uncertain parameters. Although the actual aerodynamic model of an aircraft is highly nonlinear and complicated, a simplified aerodynamic model has been widely used by control engineers because of its utility. With these concepts, a simplified model can be considered as the basis of a known structure with LSM.
Simplified aerodynamic model is defined as:

$$F_{x,Aero} = \tilde{C}_X \bar{q} S_w, \quad F_{y,Aero} = \tilde{C}_Y \bar{q} S_w, \quad F_{z,Aero} = \tilde{C}_Z \bar{q} S_w, \tag{37}$$

$$L_{Aero} = \tilde{C}_l \bar{q} S_w b, \quad M_{Aero} = \tilde{C}_m \bar{q} S_w \bar{c}, \quad N_{Aero} = \tilde{C}_n \bar{q} S_w b, \tag{38}$$

where

$$\tilde{C}_X = \tilde{C}_{X_0} + \tilde{C}_{X_\alpha}\alpha + \tilde{C}_{X_{\alpha^2}}\alpha^2 + \tilde{C}_{X_{\delta_{elv}}}\delta_{elv}, \tag{39}$$

$$\tilde{C}_Y = \tilde{C}_{Y_\beta}\beta + \tilde{C}_{Y_{\delta_{ail}}}\delta_{ail} + \tilde{C}_{Y_{\delta_{rud}}}\delta_{rud} + \tilde{C}_{Y_p}\frac{bp}{2V_T} + \tilde{C}_{Y_r}\frac{br}{2V_T}, \tag{40}$$

$$\tilde{C}_Z = \tilde{C}_{Z_0} + \tilde{C}_{Z_\alpha}\alpha + \tilde{C}_{Z_{\alpha^2}}\alpha^2 + \tilde{C}_{Z_{\delta_{elv}}}\delta_{elv} + \tilde{C}_{Z_q}\frac{\bar{c}q}{2V_T}, \tag{41}$$

$$\tilde{C}_l = \tilde{C}_{l_\beta}\beta + \tilde{C}_{l_{\delta_{ail}}}\delta_{ail} + \tilde{C}_{l_{\delta_{rud}}}\delta_{rud} + \tilde{C}_{l_p}\frac{bp}{2V_T} + \tilde{C}_{l_r}\frac{br}{2V_T}, \tag{42}$$

$$\tilde{C}_m = \tilde{C}_{m_0} + \tilde{C}_{m_\alpha}\alpha + \tilde{C}_{m_{\delta_{elv}}}\delta_{elv} + \tilde{C}_{m_q}\frac{\bar{c}q}{2V_T}, \tag{43}$$

$$\tilde{C}_n = \tilde{C}_{n_\beta}\beta + \tilde{C}_{n_{\delta_{ail}}}\delta_{ail} + \tilde{C}_{n_{\delta_{rud}}}\delta_{rud} + \tilde{C}_{n_p}\frac{bp}{2V_T} + \tilde{C}_{n_r}\frac{br}{2V_T}. \tag{44}$$

$[\tilde{C}_X, \tilde{C}_Y, \tilde{C}_Z]$ and $[\tilde{C}_l, \tilde{C}_m, \tilde{C}_n]$ are simplified force and moment coefficients of X, Y, Z axis defined in body-fixed coordinate.
To determine the simplified pitching moment coefficients $\tilde{C}_m$ using LSM, proceed as follows.
Equation (38) and Equation (43) can be rewritten as follows:

$$z = X\tilde{\theta} + \varepsilon, \tag{45}$$

where

$$z = \begin{bmatrix} \frac{I_{yy}\dot{q}(t_1)+(I_{xx}-I_{zz})r(t_1)p(t_1)}{\bar{q}(t_1)S_w\bar{c}} & \frac{I_{yy}\dot{q}(t_2)+(I_{xx}-I_{zz})r(t_2)p(t_2)}{\bar{q}(t_2)S_w\bar{c}} & \cdots & \frac{I_{yy}\dot{q}(t_m)+(I_{xx}-I_{zz})r(t_m)p(t_m)}{\bar{q}(t_m)S_w\bar{c}} \end{bmatrix}^T, \tag{46}$$

$$X = \begin{bmatrix} 1 & \alpha(t_1) & \delta_{elv}(t_1) & \frac{\bar{c}q(t_1)}{2V_T(t_1)} \\ 1 & \alpha(t_2) & \delta_{elv}(t_2) & \frac{\bar{c}q(t_2)}{2V_T(t_2)} \\ \vdots & \vdots & \vdots & \vdots \\ 1 & \alpha(t_m) & \delta_{elv}(t_m) & \frac{\bar{c}q(t_m)}{2V_T(t_m)} \end{bmatrix}, \tag{47}$$

$$\tilde{\theta} = \begin{bmatrix} \tilde{C}_{m_0} & \tilde{C}_{m_\alpha} & \tilde{C}_{m_{\delta_{elv}}} & \tilde{C}_{m_q} \end{bmatrix}^T, \tag{48}$$

$$\varepsilon = \begin{bmatrix} \varepsilon(t_1) & \varepsilon(t_2) & \cdots & \varepsilon(t_m)^T \end{bmatrix}. \tag{49}$$

The vector z and the matrix X are constructed using the measured data. Especially, the derivative term, $\dot{q}$ in z is computed with a numerical differentiation of measured angular rates, q. From an LSM perspective, the most reliable estimate of $\tilde{\theta}$ is obtained by minimizing the sum of the squared differences between the measured output z and the model output $y = X\tilde{\theta}$. Accordingly, an optimal least-squares solution that minimizes the cost function:

$$J(\tilde{\theta}) = \frac{1}{2}(z - X\tilde{\theta})^T(z - X\tilde{\theta}), \tag{50}$$

can be calculated with

$$\tilde{\theta} = (X^T X)^{-1} X^T z. \tag{51}$$

The same methodology can be applied to the estimation of other aerodynamic coefficients.

4. Data-Driven Model Discovery

4.1 Trim Point Design

The take-off and landing phases are not considered in this paper since flight simulation starts at the steady-level flight trimmed state. Through Equations (7), (8) and (25) to (30), trim point is computed in conditions: $\dot{U} = \dot{\beta} = \dot{\alpha} = \dot{\phi} = \dot{\theta} = p = q = r = 0$. Results of the trimmed condition of aircraft are given by Table 2.

Parameters	Values	Units
Altitude(h)	10,000	ft
Air Density(ρ)	0.9105	kg/m^3
Thrust(T^t)	2090	N
Airspeed($V_T{}^t$)	105	m/s
Angle of Attack(α^t)	2.395	deg
Pitch Angle(θ^t)	2.395	deg
Elevator Deflection Angle($\delta_{elv}{}^t$)	1.1	deg

Table 2 – Trimmed condition on steady-level flight.

Equation (25) to Equation (30) can be rearranged by considering α, θ, δ_{elv} as the sum of trimmed states(α^t, θ^t, $\delta_{elv}{}^t$) and perturbations:

$$\alpha = \alpha^t + \tilde{\alpha}, \quad \theta = \theta^t + \tilde{\theta}, \quad \delta_{elv} = \delta_{elv}{}^t + \tilde{\delta}_{elv}. \tag{52}$$

Using perturbations as the states instead of true states makes constant terms of (20), (22), and (26) to (30) cleared. This form of rearrangement can help to reduce the steady-state error.

4.2 Control Input Scenario Design

Appropriate control inputs play a key role in improving the performance of system identification. Especially, it has a significant impact on data-driven modeling due to its requirement for huge amount of data. In this study, we explore the optimal control input that maximally stimulates multiple attitude states while preventing the aircraft from stall. Through heuristic trial and error, the control input scenario takes the form of Figure 3.

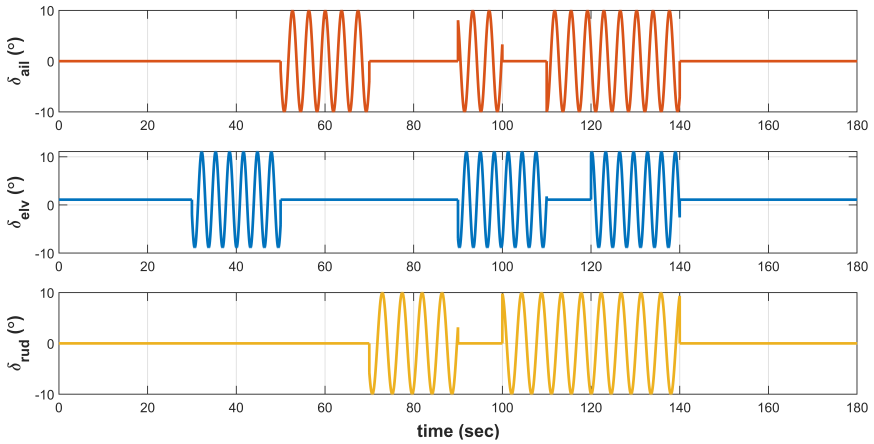

Figure 3 – Control surface deflection scenario over time for system identification.

4.3 Model Discovery with SINDy

With logged time-series data about states of $[U, \beta, \alpha, p, q, r, \phi, \theta]$ by control input in Figure 3, SINDy algorithm is defined as follows:

$$\begin{aligned} \dot{\mathbf{X}} &= [\dot{U},\ \dot{\beta},\ \dot{\tilde{\alpha}},\ \dot{p},\ \dot{q},\ \dot{r},\ \dot{\phi},\ \dot{\tilde{\theta}}], \\ \mathbf{X} &= [U,\ \beta,\ \tilde{\alpha},\ p,\ q,\ r,\ \phi,\ \tilde{\theta}],\quad \mathbf{U} = [\delta_{ail},\ \tilde{\delta}_{elv},\ \delta_{rud}], \\ \Theta(\mathbf{X},\ \mathbf{U}) &= [1,\ x_1,\ ...,\ x_8,\ u_1,\ u_2,\ u_3,\ {x_1}^2,\ x_1x_2\ ...,\ x_1x_8,\ ...,\ x_1u_3,\ ...,\ {u_3}^2,\ ...,\ x_1^3,\ ...,\ {x_8}^3,\ ...,\ u_3^3]. \end{aligned} \tag{53}$$

The fidelity of the SINDy method is demonstrated by the comparison of $\dot{\mathbf{X}}$ data between the discovered model from SINDy and the true model. The results are given in Figure 4.

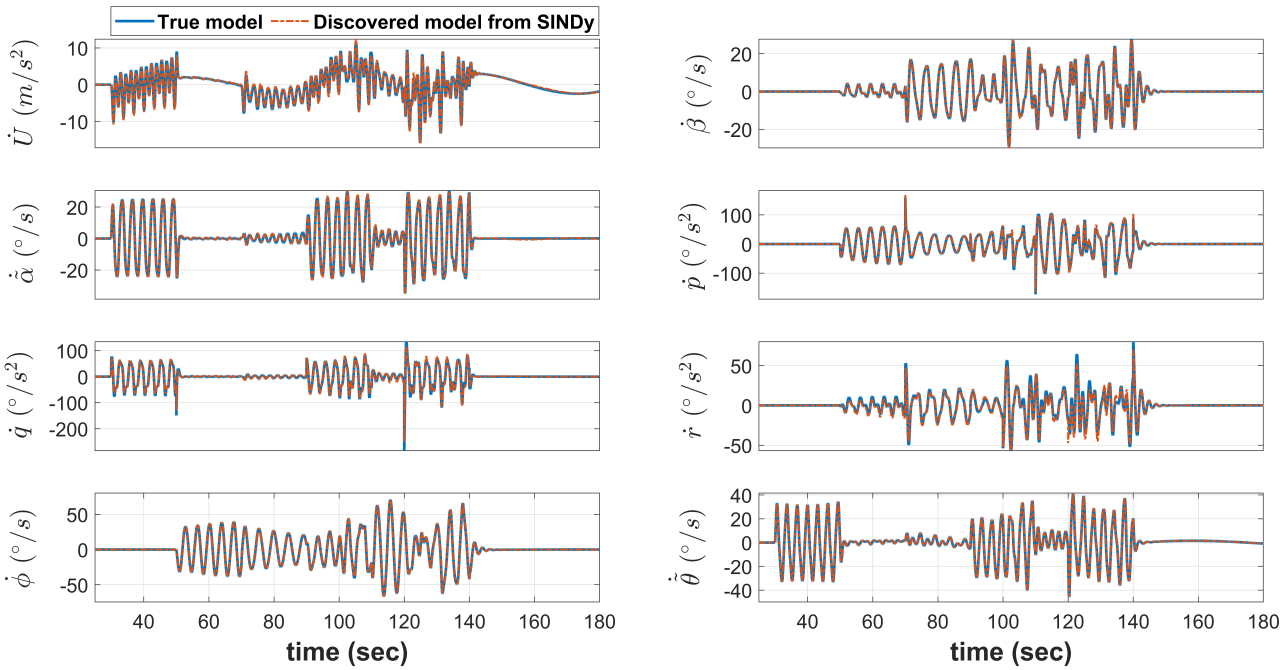

Figure 4 – State derivatives comparison between the model from SINDy and the true model.

The coefficient matrix(Ξ) results that obtained by SINDy are shown in (57) and Table 4 in Appendix A. The truncated functions are omitted from the total number of 364 candidate function terms in 57. In the process of choosing the magnitude of the regularization parameter, λ, the number of active terms is considered to be around 15. Each size of component in lambda is set manually to optimize for each state variable. The regularization parameters finally decided are as follows:

$$\lambda = [90,\ 0.62,\ 5,\ 9.8,\ 12,\ 6,\ 1.8,\ 0.4]. \tag{54}$$

4.4 Model Discovery with Least Square Method

The aerodynamic coefficients of $[\tilde{C}_X, \tilde{C}_Y, \tilde{C}_Z]$ and $[\tilde{C}_l, \tilde{C}_m, \tilde{C}_n]$ are identified by using LSM as given following Table 3.

$[\tilde{C}_{X_0},\ \tilde{C}_{X_\alpha},\ \tilde{C}_{X_{\alpha^2}},\ \tilde{C}_{X_{\delta_{elv}}}]$	[0.0208, 0.0013, 3.98e-04, -4.688e–04]
$[\tilde{C}_{Y_\beta},\ \tilde{C}_{Y_{\delta_{ail}}},\ \tilde{C}_{Y_{\delta_{rud}}},\ \tilde{C}_{Y_p},\ \tilde{C}_{Y_r}]$	[-0.0161, 0.0011, 0.0011, -0.2118, 1.9244]
$[\tilde{C}_{Z_0},\ \tilde{C}_{Z_\alpha},\ \tilde{C}_{Z_{\alpha^2}},\ \tilde{C}_{Z_{\delta_{elv}}},\ \tilde{C}_{Z_q}]$	[0.0496, 0.0915, -4.09e-04, 0.0375, 65.66]
$[\tilde{C}_{l_\beta},\ \tilde{C}_{l_{\delta_{ail}}},\ \tilde{C}_{l_{\delta_{rud}}},\ \tilde{C}_{l_p},\ \tilde{C}_{l_r}]$	[-0.001, 0.0014, -1.37e-04, -0.4959, 0.0412]
$[\tilde{C}_{m_0},\ \tilde{C}_{m_\alpha},\ \tilde{C}_{m_{\delta_{elv}}},\ \tilde{C}_{m_q}]$	[0.0523, -0.0139, -0.0176, -15.57]
$[\tilde{C}_{n_\beta},\ \tilde{C}_{n_{\delta_{ail}}},\ \tilde{C}_{n_{\delta_{rud}}},\ \tilde{C}_{n_p},\ \tilde{C}_{n_r}]$	[0.0019, 1.49e-05, -0.0018, -0.0568, -0.2943]

Table 3 – Estimated simplified aerodynamic coefficients from LSM.

In Figure 5, there is an estimation error between the true model and LSM driven model. That error is inevitable, caused by the lack of coupling terms in (39) to (44). Generally, those minor errors are considered model uncertainty and covered with the marginal design of the control system.

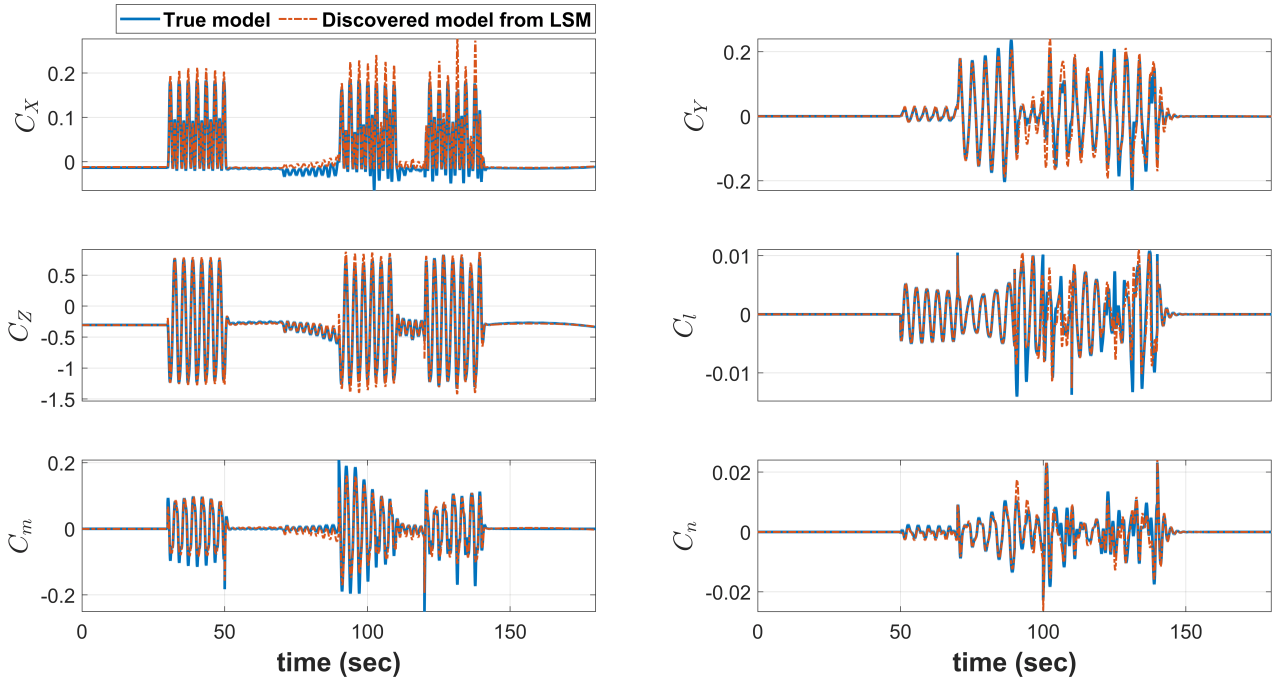

Figure 5 – Comparison of aerodynamic model between the model from LSM and the true model.

4.5 Discovered Model Validation with Control Input

Final Validation of each discovered model is performed to check the damping performance compared to the true model. The serial doublet signals are input to each control surface to check the responses of each axis. The control inputs of each surface and the results of model validation are shown in Figure 6 and Figure 7 in each.

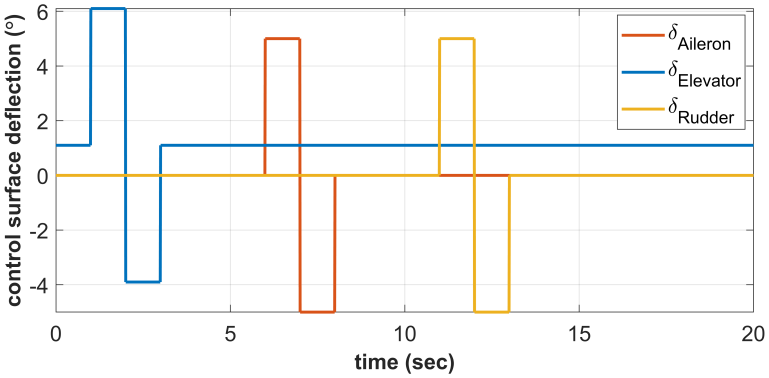

Figure 6 – Control doublet inputs for model validation.

In Figure 7, the discovered models show proper damping responses after doublet input. It is demonstrated that the discovered models from both SINDy and LSM have a high enough model fidelity to be used for control system design.

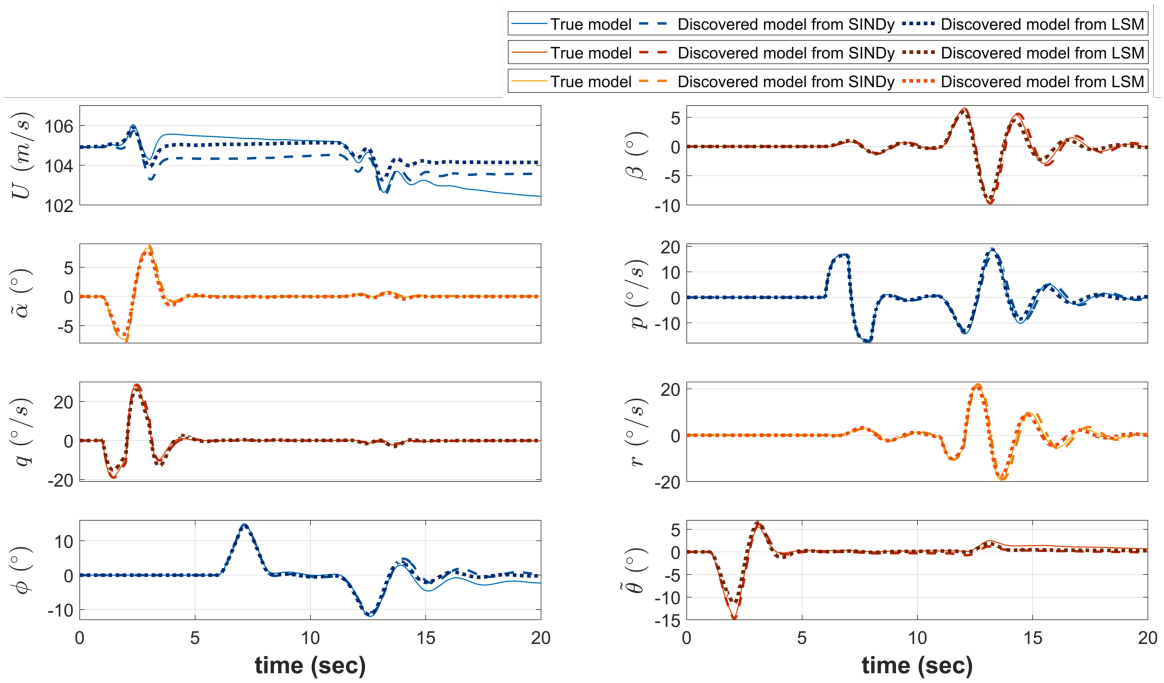

Figure 7 – States comparison of true and discovered models after doublet input.

5. Model Predictive Control

Model predictive control (MPC) has become a prominent control theory that anticipates the reference state and output within future time windows, known as the prediction horizon. In real-time implementation, finite-horizon optimization is conducted on the dynamics model to ensure the convergence of the future predicted output to the reference trajectory as follows in Figure 8. The key objective is to minimize the objective function, resulting in an optimal sequence of control inputs that consistently adhere to constraints at each time point [20, 21].

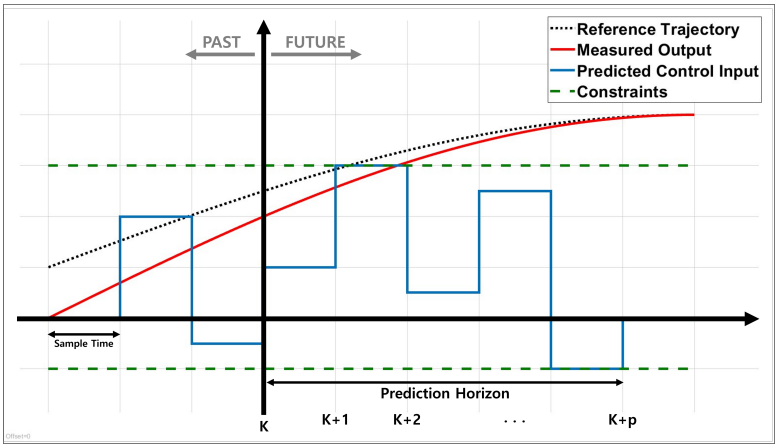

Figure 8 – Concept of model predictive control.

The combination of SINDy, which can discover the dynamics model of the system with minimal prior information, and MPC, which provides stable constraints, will show strong control performance against the uncertainties mentioned above [22, 23, 24].

5.1 Numerical Simulation

Control via NMPC is performed to verify the performance of data-driven modeling. In particular, the true model, SINDy model, and LSM model are each used for NMPC under the same conditions. The optimized inputs generated from them are fed into a simulation environment configured based on the true model to compare the fidelity between the models. The concept diagram of NMPC with the

data-driven models is shown in Figure 9.

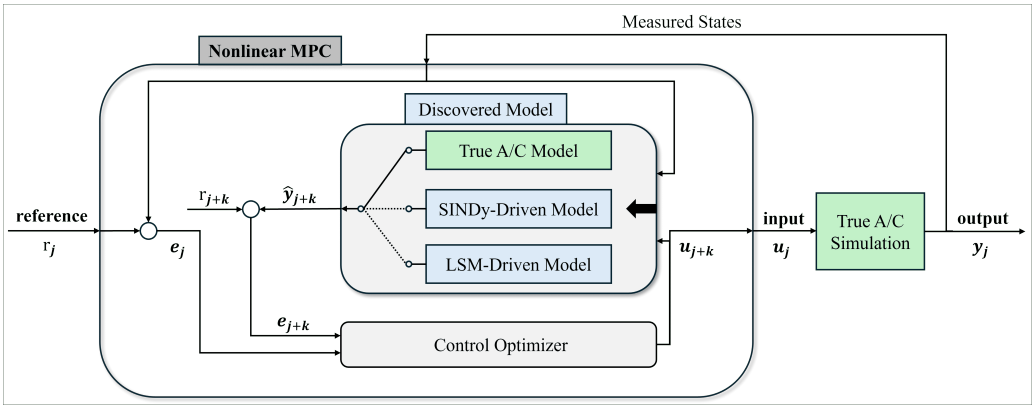

Figure 9 – Diagram of nonlinear model predictive control for data-driven model validation.

The optimal control inputs by NMPC are computed over a prediction horizon to minimize a cost function J defined as:

$$J = \mathbf{Q} \sum_{k=0}^{m_p-1} \left\| \hat{\mathbf{x}}_{j+k} - \mathbf{r}_k \right\|^2 + \mathbf{R}_{\Delta u} \sum_{k=1}^{m_c-1} \left\| \Delta \mathbf{u}_{j+k} \right\|^2, \tag{55}$$

subject to the discrete-time dynamics and constraints with time step Δt, prediction horizon $T_p = m_p \Delta t$, and control horizon $T_c = m_c \Delta t$. The cost function aims to minimize gaps between the predicted states $\hat{\mathbf{x}}$ and the reference trajectory $\mathbf{r}$, and the size of the rate of control surface deflection $\Delta \mathbf{u}$. Both of terms are weighted by $\mathbf{Q}, \mathbf{R}_{\Delta u}$ matrices each.
The detailed parameters for NMPC are set as follows:

$$\begin{aligned} &\hat{\mathbf{x}} = [U,\ \beta,\ \tilde{\alpha},\ p,\ q,\ r,\ \phi,\ \tilde{\theta}]^T, \mathbf{u} = [\delta_{ail},\ \tilde{\delta}_{elv},\ \delta_{rud}]^T, m_p = 15,\ \ m_c = 15,\ \ \Delta t = 0.1\text{s}, \\ &\mathbf{Q} = diag(0,\ 0,\ 0,\ 0,\ 0,\ 0,\ 3,\ 3),\ \ \mathbf{R}_{\Delta u} = diag(0.002,\ 0.002,\ 0.002), \\ &Constraints = \begin{cases} |\alpha| < 20^\circ,\ |\beta| < 10^\circ,\ |\theta| < 45^\circ \\ |\delta_{ail}| < 25^\circ,\ |\delta_{elv}| < 25^\circ,\ |\delta_{rud}| < 25^\circ \end{cases} \end{aligned} \tag{56}$$

with an initial condition as the trimmed condition in Table 2.
The reference trajectory is designed to reflect the target aircraft's high-maneuver characteristics appropriately. The optimized control inputs of each surface and the output states through NMPC are shown in Figures 10 and 11.

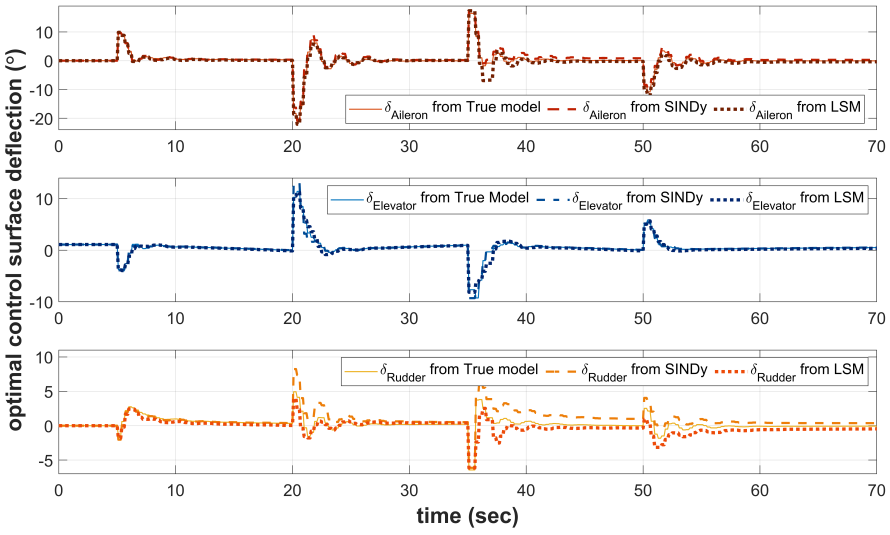

Figure 10 – Optimized control inputs for nonlinear model predictive control.

In Figure 11, both of the models from SINDy and LSM perform well enough to be used as a target model for NMPC compared to the true model. Nonetheless, due to the absence of coupling terms, the SINDy model performs more like the true model case in the region where the model is highly nonlinear. This leads to a difference in settling time in the longitudinal axis between the SINDy model and the LSM model. The difference of overshoot percentage in the lateral axis is observed either.

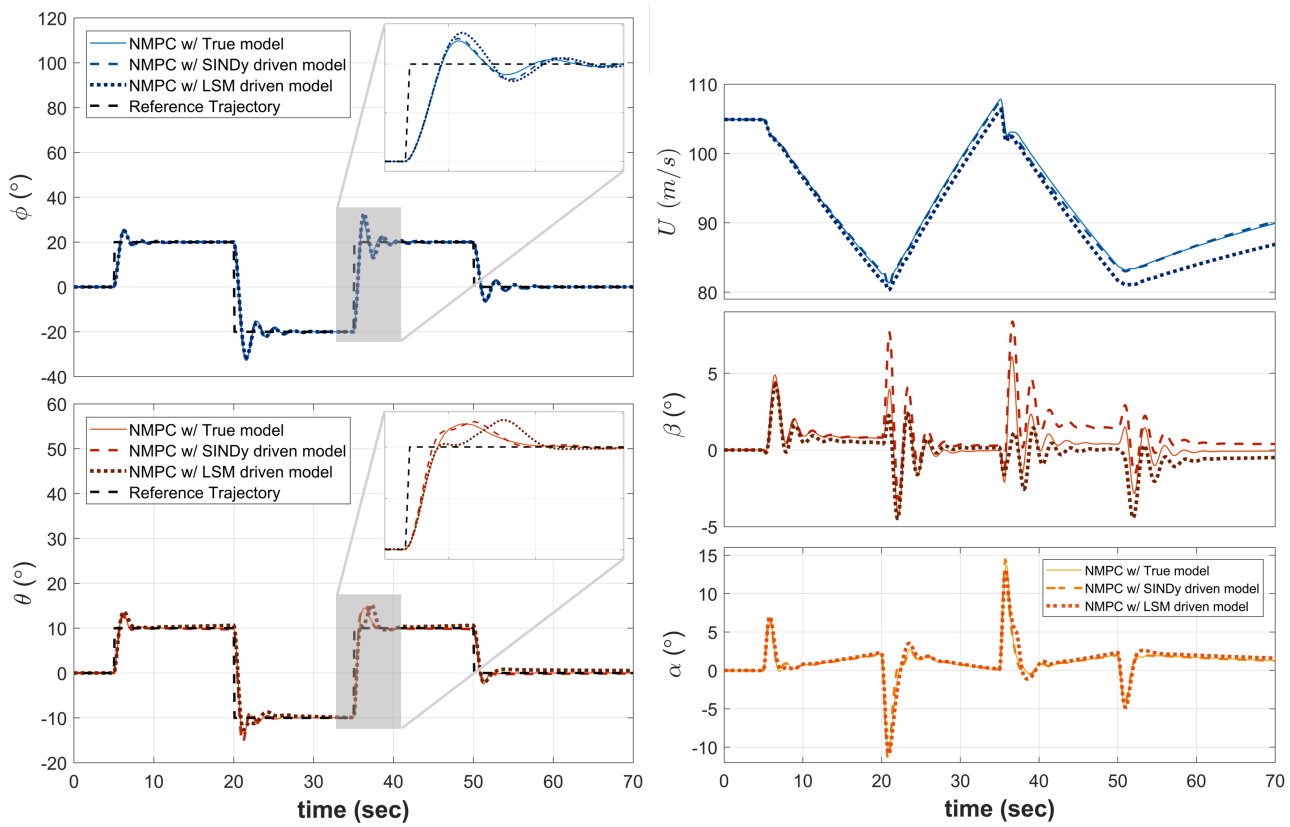

Figure 11 – Output states through nonlinear model predictive control with true model, SINDy driven model, and LSM driven model.

6. Conclusions

The methodology for discovering nonlinear dynamics of aircraft using SINDy and LSM with measured state variable data is proposed to implement NMPC. By comparing SINDy and LSM, SINDy shows good prediction performance by considering the nonlinear coupling effect so that SINDy shows improvement in control performance. This demonstrates that SINDy is a proper method of modeling nonlinear near-stall envelopes for fixed-wing aircraft, especially for high-performance trainer aircraft. Only, all the above research was performed without consideration of system dynamics such as model delay, measurement noise, and native sensor errors. Therefore, a follow-up study could be done to obtain similar simulation results with a system model and noise.

7. Acknowledgements

This research was supported by the South Korean Government (915094103).

8. Copyright Statement

References

[1] Bommanahal M and Goman M. Nonlinear unsteady aerodynamic modeling by volterra variational approach. In *AIAA Atmospheric Flight Mechanics Conference*, page 4654, 2012.

[2] Planeaux J and Barth T. High-angle-of-attack dynamic behavior of a model high-performance fighter aircraft. In *15th Atmospheric Flight Mechanics Conference*, page 4368, 1988.

[3] Tol HJ, de Visser CC, Sun LG, van Kampen E, and Chu QP. Multivariate spline-based adaptive control of high-performance aircraft with aerodynamic uncertainties. *Journal of Guidance, Control, and Dynamics*, 39(4):781–800, 2016.

[4] Donald G and William S. Some problems concerning wind tunnel testing of automotive vehicles. *SAE Transactions*, pages 593–607, 1967.

[5] Hosain ML and Fdhila RB. Literature review of accelerated cfd simulation methods towards online application. *Energy Procedia*, 75:3307–3314, 2015.

[6] Brunton SL, Kutz JN, Manohar K, Aravkin AY, Morgansen K, Klemisch J, Goebel N, Buttrick J, Poskin J, Blom-Schieber AW, and Hogan T. Data-driven aerospace engineering: reframing the industry with machine learning. *AIAA Journal*, 59(8):2820–2847, 2021.

[7] Brunton SL and Kutz JN. *Data-driven science and engineering: Machine learning, dynamical systems, and control*. Cambridge University Press, 2022.

[8] Chu SR, Shoureshi R, and Tenorio M. Neural networks for system identification. *IEEE Control systems magazine*, 10(3):31–35, 1990.

[9] Kocijan J, Girard A, Banko B, and Murray-Smith R. Dynamic systems identification with gaussian processes. *Mathematical and Computer Modelling of Dynamical Systems*, 11(4):411–424, 2005.

[10] Lee JD, Kim LS, Zewge NS, and Bang HC. Fault-tolerant control for aircraft with structural damage using sparse online gaussian process regression. *International Journal of Aeronautical and Space Sciences*, 2024.

[11] Kaiser E, Kutz JN, and Brunton SL. Data-driven discovery of koopman eigenfunctions for control. *Machine Learning: Science and Technology*, 2(3):035023, 2021.

[12] Morelli EA. Determining aircraft moments of inertia from flight test data. *Journal of Guidance, Control, and Dynamics*, 45(1):4–14, 2022.

[13] Brunton SL, Proctor JL, and Kutz JN. Discovering governing equations from data by sparse identification of nonlinear dynamical systems. *Proceedings of the National Academy of Sciences*, 113(15):3932–3937, 2016.

[14] Thibodeaux TW. *Data-driven system identification of nonlinear dynamics for a 6-DOF aircraft model using SINDYc*. PhD thesis, Wichita State University, 2019.

[15] Matpan H. Data driven model discovery and control of longitudinal missile dynamics. Master's thesis, Middle East Technical University, 2021.

[16] Brunton SL, Proctor JL, and Kutz JN. Sparse identification of nonlinear dynamics with control (sindyc). *IFAC-PapersOnLine*, 49(18):710–715, 2016.

[17] Jayden Dongwoo Lee, Sukjae Im, and Hyochoong Bang. Data-driven fault detection and isolation for quadrotor using sparse identification of nonlinear dynamics and thau observer. In *2024 International Conference on Unmanned Aircraft Systems (ICUAS)*, pages 382–389, 2024.

[18] Durham W. *Aircraft flight dynamics and control*. John Wiley & Sons, 2013.

[19] Paul J. *Jane's all the world's aircraft. 2004-2005*. Jane's Information Group Inc, Alexandria, 2005.

[20] Morari M and Lee JH. Model predictive control: past, present and future. *Computers & chemical engineering*, 23(4-5):667–682, 1999.

[21] Eren U, Prach A, Koçer BB, Raković SV, Kayacan E, and Açıkmeşe B. Model predictive control in aerospace systems: Current state and opportunities. *Journal of Guidance, Control, and Dynamics*, 40(7):1541–1566, 2017.

[22] Fasel U, Kaiser E, Kutz JN, Brunton BW, and Brunton SL. Sindy with control: A tutorial. In *2021 60th IEEE Conference on Decision and Control (CDC)*, pages 16–21, 2021.

[23] Kaiser E, Kutz JN, and Brunton SL. Sparse identification of nonlinear dynamics for model predictive control in the low-data limit. *Proceedings of the Royal Society A*, 474(2219):20180335, 2018.

[24] Abdullah F and Christofides PD. Real-time adaptive sparse-identification-based predictive control of nonlinear processes. *Chemical Engineering Research and Design*, 196:750–769, 2023.

9. APPENDIX A

$$
\begin{aligned}
\Theta(U) &= [\tilde{\alpha},\ \delta_{rud},\ U\tilde{\alpha},\ Uq,\ U\tilde{\theta},\ U\delta_{rud},\ \tilde{\alpha}\tilde{\delta}_{elv},\ U^2\tilde{\theta},\ U^2\delta_{rud},\ U\beta r,\ U\tilde{\alpha}^2,\ U\tilde{\alpha}q,\ U\tilde{\alpha}\tilde{\delta}_{elv}],\\
\Theta(\beta) &= [p,\ r,\ \phi,\ U\beta,\ U\phi,\ \tilde{\alpha}p,\ p\delta_{rud},\ \phi\delta_{rud},\ \delta_{ail}\delta_{rud},\ {\delta_{rud}}^2,\ U^2\phi,\ Up\delta_{rud},\ U\phi\delta_{rud},\ U\delta_{ail}\delta_{rud},\ U{\delta_{rud}}^2],\\
\Theta(\tilde{\alpha}) &= [\tilde{\alpha},\ q,\ \tilde{\delta}_{elv},\ U^2,\ U\tilde{\alpha},\ U\tilde{\delta}_{elv},\ \beta p,\ \tilde{\alpha}\phi,\ q\phi,\ \phi\tilde{\delta}_{elv},\ U^3,\ U^2\tilde{\alpha},\ U^2q,\ U^2\tilde{\delta}_{elv},\ U\tilde{\alpha}\phi,\ Uq\phi,\ U\phi\tilde{\delta}_{elv}],\\
\Theta(p) &= [\beta,\ \delta_{ail},\ U\beta,\ Up,\ U\delta_{ail},\ \beta\tilde{\alpha},\ \tilde{\alpha}\delta_{rud},\ U^2\beta,\ U^2\delta_{ail},\ U^2\delta_{rud},\ U\beta\tilde{\alpha},\ U\tilde{\alpha}\delta_{rud},\ \beta\tilde{\alpha}^2,\ q\tilde{\delta}_{elv}\delta_{rud},\ \tilde{\delta}^2_{elv}\delta_{rud}],\\
\Theta(q) &= [\tilde{\alpha},\ q,\ \tilde{\theta},\ U\tilde{\alpha},\ Uq,\ U\tilde{\theta},\ U\tilde{\delta}_{elv},\ U^2q,\ U^2\tilde{\theta},\ U^2\tilde{\delta}_{elv},\ \tilde{\alpha}^3,\ \tilde{\alpha}^2\tilde{\delta}_{elv},\ \tilde{\alpha}\tilde{\delta}^2_{elv}],\\
\Theta(r) &= [p,\ \delta_{ail},\ \delta_{rud},\ U\beta,\ Up,\ U\delta_{ail},\ U\delta_{rud},\ q\delta_{rud},\ \tilde{\delta}_{elv}\delta_{rud},\ U^2\beta,\ U^2p,\ U^2r, U^2\delta_{ail},\ U^2\delta_{rud},\ Uq\delta_{rud},\ U\tilde{\delta}_{elv}\delta_{rud},\ \beta^3],\\
\Theta(\phi) &= [p,\ \delta_{ail},\ U\delta_{ail},\ \beta^2,\ \beta\delta_{rud},\ \tilde{\alpha}r,\ r\tilde{\theta},\ {\delta_{rud}}^2,\ U^2\delta_{ail},\ U\beta^2,\ U\beta\delta_{rud},\ U\tilde{\alpha}r,\ U{\delta_{rud}}^2,\ q\phi\tilde{\theta}],\\
\Theta(\tilde{\theta}) &= [q,\ \tilde{\delta}_{elv},\ U\tilde{\delta}_{elv},\ \tilde{\alpha}q,\ \tilde{\alpha}\tilde{\delta}_{elv},\ q^2,\ q\tilde{\delta}_{elv},\ r\phi,\ U^2q,\ U^2\tilde{\delta}_{elv},\ U\tilde{\alpha}q,\ U\tilde{\alpha}\tilde{\delta}_{elv},\ Uq^2,\ Uq\tilde{\delta}_{elv},\ q\phi^2].
\end{aligned}
\tag{57}
$$

$\Xi = [\xi_1\ \xi_2\ \xi_3\ \xi_4\ \xi_5\ \xi_6\ \xi_7\ \xi_8]$								
	ξ_1	ξ_2	ξ_3	ξ_4	ξ_5	ξ_6	ξ_7	ξ_8
$\xi_O(1)$	-8.551	0.049	3.5577	1.6878	11.0379	1.8315	0.9996	0.9753
$\xi_O(2)$	0.227	-0.9799	0.4714	-0.0592	-2.6068	-0.071	-0.0079	9.29e-04
$\xi_O(3)$	0.153	0.3573	0.0436	-0.0303	-1.1706	0.022	1.45e-04	-5.31e-05
$\xi_O(4)$	-0.041	-0.0022	1.27e-05	-0.043	-0.1816	-0.0126	-3.8856	0.2737
$\xi_O(5)$	-0.201	-0.0047	-0.0906	0.0014	0.0256	-0.037	0.1257	0.0178
$\xi_O(6)$	-0.0046	0.974	-0.0015	15.598	0.0246	0.0015	-1.4878	-0.0425
$\xi_O(7)$	1.205	-0.0035	-0.9527	-0.1873	-5.49e-04	-1.52e-04	0.9331	-0.0027
$\xi_O(8)$	0.0011	0.0058	1.4075	-6.75e-04	-2.2e-04	0.2324	-8.25e-04	-0.93
$\xi_O(9)$	2.25e-05	-2.48e-04	1.067	1.83e-05	-1.28e-04	0.01	-6.42e-07	2.08e-06
$\xi_O(10)$	1.086	-2.41e-04	0.0799	-4.74e-06	-2.34e-05	6.92e-04	0.0397	4.23e-07
$\xi_O(11)$	0.734	1.917e-05	-1.21e-07	-0.4947	-110.5	1.693e-04	-0.0014	-0.0023
$\xi_O(12)$	-1.042	4.59e-05	3.96e-04	0.0038	-1.007	-6.88e-05	0.0156	-1.69e-04
$\xi_O(13)$	-0.0172	-6.01e-05	3.671e-05	-56.65	-0.023	-7.04e-06	9.89e-06	4.99e-04
$\xi_O(14)$	-	-3.27e-06	9.35e-06	-0.009	-	-1.04e-05	1.0095	3.46e-05
$\xi_O(15)$	-	3.08e-06	-0.014	-4.84e-04	-	-0.0016	-	-0.479
$\xi_O(16)$	-	-	-0.01	-	-	-4.02e-05	-	-
$\xi_O(17)$	-	-	-7.57e-04	-	-	21.99	-	-

Table 4 – Sparse coefficient matrix.